Biomacromolecules

pubs.acs.org/Biomac

Article

Enzyme-Functionalized Cellulose Beads as a Promising Antimicrobial Material

Davide Califano, Bethany Lee Patenall, Marco A.S. Kadowaki, Davide Mattia, Janet L. Scott, and Karen J. Edler*

Cite This: *Biomacromolecules* 2021, 22, 754–762

Read Online

ACCESS | Metrics & More | Article Recommendations | Supporting Information

ABSTRACT: The extensive use of antibiotics over the last decades is responsible for the emergence of multidrug-resistant (MDR) microorganisms that are challenging health care systems worldwide. The use of alternative antimicrobial materials could mitigate the selection of new MDR strains by reducing antibiotic overuse. This paper describes the design of enzyme-based antimicrobial cellulose beads containing a covalently coupled glucose oxidase from *Aspergillus niger* (GOx) able to release antimicrobial concentrations of hydrogen peroxide (H_2O_2) (≈ 1.8 mM). The material preparation was optimized to obtain the best performance in terms of mechanical resistance, shelf life, and H_2O_2 production. As a proof of concept, agar inhibition halo assays (Kirby-Bauer test) against model pathogens were performed. The two most relevant factors affecting the bead functionalization process were the degree of oxidation and the pH used for the enzyme binding process. Slightly acidic conditions during the functionalization process (pH 6) showed the best results for the GOx/cellulose system. The functionalized beads inhibited the growth of all the microorganisms assayed, confirming the release of sufficient antimicrobial levels of H_2O_2. The maximum inhibition efficiency was exhibited toward *Pseudomonas aeruginosa* (*P. aeruginosa*) and *Escherichia coli* (*E. coli*), although significant inhibitory effects toward methicillin-resistant *Staphylococcus aureus* (MRSA) and *S. aureus* were also observed. These enzyme-functionalized cellulose beads represent an inexpensive, sustainable, and biocompatible antimicrobial material with potential use in many applications, including the manufacturing of biomedical products and additives for food preservation.

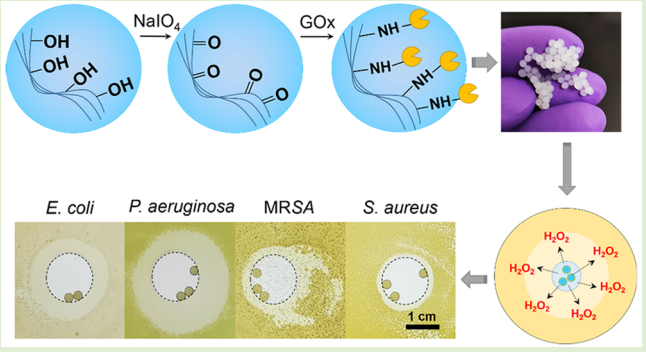

INTRODUCTION

Decades of extensive use of antibiotics have led to the emergence of multidrug-resistant (MDR) bacterial strains, considered as one of the most significant threats to human health worldwide.[1,2] For example, methicillin-resistant *Staphylococcus aureus* (MRSA) alone, each year, kills more Americans than HIV, Parkinson's disease, and homicide.[3] MDR bacteria associated with wound biofilms are particularly concerning, owing to bacterial biofilms requiring between 4 and 1000 times higher concentrations of antibiotics for eradication,[4] especially in patients with chronic pathologies such as diabetes, cancer, or vascular diseases.[5] To mitigate against the selection of additional MDR strains, it is essential to reduce antibiotic overuse, principally in those cases where infection prevention is achieved through antibiotic prophylaxis.[6] One strategy to reduce the risk of infection in wounds is the use of antimicrobial substances, an alternative to antibiotics, which do not trigger the selection of resistance traits in microorganisms.[7] Hydrogen peroxide (H_2O_2) has a wide range of efficacy against viruses, bacteria, and fungi, which makes it one of the most commonly used biocidal compounds.[8,9] H_2O_2 triggers an oxidative cascade reaction able to cause DNA damage, major disruption in protein synthesis, and to phospholipid membrane arrangement.[10] Moreover, even low concentrations of H_2O_2 (at the micromolar level) play a role in redox-sensitive cell signaling, which can improve dermal healing while inhibiting the growth of some bacteria.[11,12] For this reason, H_2O_2-producing enzymes have been investigated for potential use as a sustainable alternative to antibiotics.[13] Among these, glucose oxidase (GOx) from *Aspergillus niger* catalyzes the oxidation of *β*-D-glucose using molecular oxygen, producing H_2O_2 and gluconic acid.[14] The combination of oxygen consumption and media acidification, owing to the generation of gluconic acid and the production of H_2O_2, make GOx applicable for antimicrobial

Received: October 26, 2020
Revised: December 11, 2020
Published: January 6, 2021

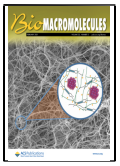

Scheme 1. General Approach to Creation of the Enzyme-Functionalized Dialdehyde Cellulose Beads[a]

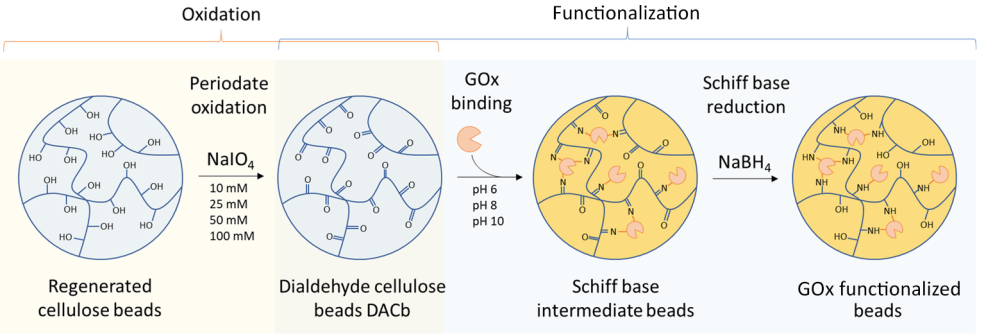

[a]Details are provided in the Experimental Section.

purposes.[15] However, the use of free enzymes in solution presents critical disadvantages for many industrial applications such as high separation costs and reduced stability.[16,17] In contrast, the immobilization of the enzymes into a suitable material may increase the stability in a wider range of conditions, confine the activity to a specific area, and mitigate enzyme deactivation upon storage.[16] For these reasons, the use of immobilized enzymes as biocatalysts is particularly appealing. Cellulose/chitosan composite beads were employed for the immobilization of lipases, showing the feasibility of biopolymers as support materials.[18] The use of cellulose as a support (both native and derivatized) for enzyme immobilization has been well established in a wide range of biomedical applications,[19] owing to its biodegradability, low cost, and biocompatibility.[20] The presence of hydroxyl moieties in cellulose can be used to add functional groups able to make the immobilization of GOx feasible.[21,22] Periodate mediated cellulose oxidation generates aldehyde moieties that can be used to bind the enzyme lysines *via* imine formation, also known as a Schiff base.[20] This well-established binding method has been used for the immobilization of proteins and enzymes on cellulose-based materials.[23−25] The general approach to the creation of the GOx-functionalized beads herein used is shown in Scheme 1. Details are provided in the Experimental Section below. This study explores the preparation of an enzyme/cellulose hydrogel composite, in the form of beads, and its manufacturing optimization. In particular, the effect of pH on the enzyme binding affinity and activity retention upon storage was explored. In addition, the antimicrobial efficacy of GOx-functionalized beads against four important nosocomial bacterial strains (two Gram-negative and two Gram-positive) was determined by *in vitro* assays (adapted Kirby-Bauer test).

EXPERIMENTAL SECTION

Chemicals and Strains. *Materials.* Absolute ethanol (VWR Chemicals, ≥ 99.8), hydroxylamine hydrochloride (159417, Sigma-Aldrich, ≥ 99%), sodium hydroxide (1.06498, Supelco, ≥ 99.0%), hydrogen peroxide 30 wt % (VWR Chemicals), glucose oxidase from *Aspergillus niger* (G7141, Sigma-Aldrich) (GOx), horseradish peroxidase ∼150 U/mg (77332, Sigma-Aldrich), bovine serum albumin (05470, Sigma-Aldrich, ≥ 96%), Bradford reagent (B6916, Supelco), D-(+)-glucose (G8270, Sigma-Aldrich, ≥ 99,5%), microcrystalline cellulose (435236, Sigma-Aldrich, LOT #MKCF1486), sodium borohydride (MFCD00003518, Acros Organics, ≥ 98%), sodium periodate (MFCD00003534, Acros Organics, ≥ 98,8%), sodium iodide (383112 Sigma-Aldrich, ≥ 99.5%), sodium acetate (S2889 Sigma-Aldrich, ≥ 99%), acetic acid (320099, Sigma-Aldrich, ≥ 99.7%), sodium phosphate dibasic (S9763, Sigma-Aldrich, ≥ 99%), sodium phosphate monobasic (S3139, Sigma-Aldrich), sodium carbonate (S7795, Sigma-Aldrich, ≥ 98%), sodium bicarbonate (S5761, Sigma-Aldrich, ≥ 99.5%), 1-ethyl-3-methylimidazloium acetate [EMIm][OAc] (BASF Basionics, ≥ 95%), and DMSO (Alfa Aesar, ≥ 99%) were all used as received unless otherwise stated.

Bacterial Strains and Growth Conditions. Methicillin-resistant *Staphylococcus aureus* (MRSA252), *Staphylococcus aureus* (strain H560), *Pseudomonas aeruginosa* (strain PAO1), and *Escherichia coli* (strain NCTC 10418) were obtained from the Jenkins Group Collection at the University of Bath. The bacterial strains were maintained on 15% (v/v) glycerol stock at −80 °C and plated onto Luria−Bertani (LB) agar for *P. aeruginosa* and *E. coli* and tryptic soy agar (TSA) for MRSA and *S. aureus*, as required to attain single colonies. To attain an overnight (ON) culture, a single colony from each culture was inoculated into 10 mL of LB broth for *P. aeruginosa* and *E. coli* and tryptic soy broth (TSB) for MRSA and *S. aureus*. Broth cultures were grown at 37 °C for 18 h with 200 rpm shaking.

Agar Inhibition Halo Test (Kirby-Bauer Test). The ON culture was grown as previously mentioned. Cultures were washed with phosphate buffered saline (PBS) (pH 7.4, 25 °C), and a subculture was made by diluting ON 1000-fold into fresh PBS. The subculture (500 μL) was inoculated onto agar, previously prepared by adding 20 mL of agar into a dish, and 12 mm diameter holes were bored into the middle of the agar gel. The desired number of functionalized beads in 200 μL of phosphate buffer (pH 6, 25 mM) either supplemented with glucose 1 wt % or without glucose, were then added to the holes. Plates were incubated statically for 18 h at 37 °C. The zone of clearance was measured *via* image analysis and normalized through the deduction of the surface in square millimeters of the central well. Image analysis was conducted using ImageJ.[26]

Preparation of Dialdehyde Cellulose Beads (DACbs). *Cellulose Dissolution.* To prepare a ∼8 wt % cellulose solution, 20 g of microcrystalline cellulose (MCC) was first dispersed in 158.5 g of dimethyl sulfoxide (DMSO) with an overhead stirrer (900 rpm) at room temperature; then, 66.5 g of 1-ethyl-3-methylimidazolium acetate ([EMIm][OAc]) was added dropwise into the dispersion, and the mixture was stirred for 4 h. The solvent ratio of DMSO/[EMIm][OAc] is 70/30 w/w.

Bead Formation and Purification. The cellulose solution (8 wt %) was dropped from a 1.2 mm × 38 mm stainless steel needle into absolute ethanol using a syringe pump (KdScientific -210) set to a constant flow rate, such that individual droplets formed. The beads were Soxhlet extracted with ethanol at 80 °C for at least 24 h to remove residual DMSO and [EMIm][OAc]. A solvent exchange into deionized water (DI) was achieved by soaking the beads in abundant DI water with at least three solvent replacements (the removal of ethanol is critical as enzyme conformation can be affected by the presence of denaturing agents).

Cellulose Bead Oxidation. The cellulose beads (10 g) were suspended in 40 mL of sodium periodate ($NaIO_4$) at different concentrations (10, 25, 50, and 100 mM) and reacted at 25 °C for 2 h under mild agitation. After the reaction, in order to remove the excess of $NaIO_4$, the beads were separated using a stainless steel sieve and washed with deionized (DI) water until the absorption of supernatant

https://dx.doi.org/10.1021/acs.biomac.0c01536
Biomacromolecules 2021, 22, 754−762

Table 1. Degree of Oxidation of Cellulose in Relation with the Periodate Concentration in the Reaction Vessel and Periodate/Cellulose Molar Ratio

sample code	$NaIO_4$ concentration (mM)	$NaIO_4$/cellulose ratio(mol/mol)	degree of oxidation (%)[a]	standard deviation
DACb-10	10	0.07	4.13	0.30
DACb-25	25	0.17	7.42	0.50
DACb-50	50	0.34	11.20	0.93
DACb-100	100	0.68	19.56	1.32

[a]Degree of oxidation is expressed in moles of carbonyls per mole of anhydrous glucose units (AUG) as a percentage. The highest degree of oxidation (100%) corresponds to a degree of substitution (DS) equal to 2 as periodate can oxidize only vicinal diols. Thus, only two out of three hydroxyl groups for each AUG can be oxidized.

at 290 nm was zero (periodate adsorption peak). The oxidized beads were stored in DI water at 4 °C.

Bead Characterization. *Oxidation Degree Determination.* Carbonyl groups were quantified by titrating HCl that was liberated as a consequence of the oximation reaction of hydroxylamine hydrochloride with carbonyls as described previously.[27] The oxidized beads (2 g of wet weight) were homogenized with 3 mL of DI water using an Ultraturrax homogenizer and dispersed into 25 mL of a 0.25 M hydroxylamine hydrochloride solution in an acetate buffer (adjusted with 0.1 M NaOH to pH 4). The HCl released in the reaction between the aldehydes and hydroxylamine hydrochloride was titrated against 0.1 M NaOH using an Accumet pH meter (Fisher Scientific), and equivalent points peaks were obtained from the first order derivative of pH changes against volume added (dpH/dV).

Uniaxial Deformation Test. To test the mechanical stability, single beads were uniaxially compressed using a stress-controlled rheometer (Discovery HR3, TA Instruments) equipped with a 12 mm plate geometry. The beads were uniaxially compressed at a constant deformation rate of 6 μm/s. The strain (Y_a) was calculated as the fraction of sample deformation, and the distance corresponding to the sample height was obtained at the point where the axial force starts to increase (eq 1),

$$Y_a = \frac{K_s - K_{max}}{K_p} \quad (1)$$

where K_s is the sample compression, K_{max} is the maximum compression, and K_p is the sample height. The recorded axial force (N) over Y_a was used as a metric for a comparison for beads with different degrees of oxidation after their exposure to different pH values (occurred during protein binding).

Scanning Electron Microscopy. Micrographs were obtained using a JEOL SEM648OLV microscope. The samples were flash frozen in liquid nitrogen and lyophilized using a MiniLyotrap (LTE scientific). Cross sections were prepared by cutting with sharp blades before the flash freezing process. Prior to imaging, the samples were gold coated (Edwards sputter coater, S150B) for 5 min.

GOx Binding in DACb. For isotherm binding experiments, aliquots of three beads, for each degree of oxidation, were immersed and incubated (in a static manner) at 4 °C for 18 h in 50 μL of GOx solutions at different concentrations. In order to test the binding at different pH values, GOx was solubilized in different buffered solutions: phosphate buffer pH 6 (0.1 M); phosphate buffer pH 8 (0.1 M); carbonate buffer pH 10 (0.1 M). The protein concentrations were determined before and after binding using the Bradford method.[28] Calibration curves were obtained using known concentrations of GOx determined *via* UV absorption at 280 nm (molar extinction coefficient and molecular weight at 96845 M^{-1} cm^{-1} and 84004 Da, respectively). The amount of protein bound was expressed in micrograms of GOx per milligram of dry cellulose and plotted against GOx concentration in the supernatant after binding. In order to obtain isotherm binding constants, a linear eq (eq 2) was used to fit the experimental data,[29]

$$C_s = C_f K_h \quad (2)$$

where C_s is protein bound per milligram of dry cellulose, K_h is affinity constant, and C_f is concentration of free protein. To complete the immobilization process, each bead aliquot was first treated with 150 μL of $NaBH_4$ (50 mM) for 30 min at room temperature and then transferred to phosphate buffer (0.1 M pH 6) and stored at 4 °C prior to other experiments. In order to determine the relative content of proteins bound, the functionalized beads were stained *in situ*. One functionalized bead (after binding and reduction steps) was incubated in 200 μL of Bradford reagent for 30 min and photographed in a light box. The image analysis for evaluating the relative amount of proteins in the DACb was conducted using ImageJ.[26]

Release of H_2O_2 from Functionalized Beads. The activity of the functionalized beads was determined by quantifying H_2O_2 release over time. The production of H_2O_2 was conducted by immersing one functionalized bead in 10 mL of phosphate buffer (25 mM; pH 6) containing D-(+)-glucose (1 wt %) at 37 °C for 24 h under agitation (250 rpm) in an orbital shaker incubator (ES-20 grant-bio). The quantification of H_2O_2 was performed using a method previously described[30] and slightly modified. Aliquots of H_2O_2 were withdrawn and diluted with Milli-Q water (when necessary) to a concentration between 0.01 and 0.8 mM in a final volume of 50 μL. The H_2O_2 aliquots were mixed then with 50 μL of acetate buffer (0.5 M; pH 4.8) and 100 μL of 1 M sodium iodide; the mixture was incubated for 30 min, and the absorbance at 350 nm was recorded using a FLUOstar Omega Microplate Reader (BMG LABTECH) in a 96-well plate. Calibration curves were prepared by adding a known amount of H_2O_2 that had been previously titrated against potassium permanganate.[31] The functionalized beads used in this experiment were prepared using the same initial GOx concentration (1.4 mg/mL) and three different pH values (6, 8, and 10). The immobilization process was performed, as for the isotherm binding experiments, overnight in a static manner at 4 °C. In order to minimize differences in the amount of protein present in single beads, the enzyme binding was performed in a single batch (30 beads in 0.5 mL at each pH). All the experiments were conducted in triplicate, using three independent samples.

RESULTS AND DISCUSSION

Dialdehyde Cellulose Bead (DACb) Preparation and Characterization. The cellulose beads were prepared by dropping an 8 wt % cellulose solution (in a mixture of ionic liquid and DMSO) from a syringe needle into an ethanol bath in which phase inversion occurred. The cellulose beads presented a spheroidal shape and fairly narrow diameter distribution (2.46 ± 0.15 mm, determined by 30 measurements using a micrometer calibrated microscope slide). To produce dialdehyde cellulose beads (DACbs), sodium periodate was used as oxidant to open vicinal diols present on the glucopyranose units. The degree of oxidation (DO) was linearly correlated to the concentration of sodium periodate used for the reaction (Table 1).

After the reaction with sodium periodate, the average bead size decreased in DACb-100 (~16% in diameter) while the cellulose dry weight increased (~0.8 wt %) (Figure S1), suggesting that a rearrangement of the cellulose fibrils occurred upon periodate oxidation. It has been reported that the glucopyranose ring opening causes a disturbance in the

https://dx.doi.org/10.1021/acs.biomac.0c01536
Biomacromolecules 2021, 22, 754−762

crystalline order, increasing the flexibility of the nanofibrils, hence resulting in a densified network.[32,33] However, a closer observation of the internal structure of the freeze-dried DACbs revealed the presence of larger pores as the DO increased (Figure 1).

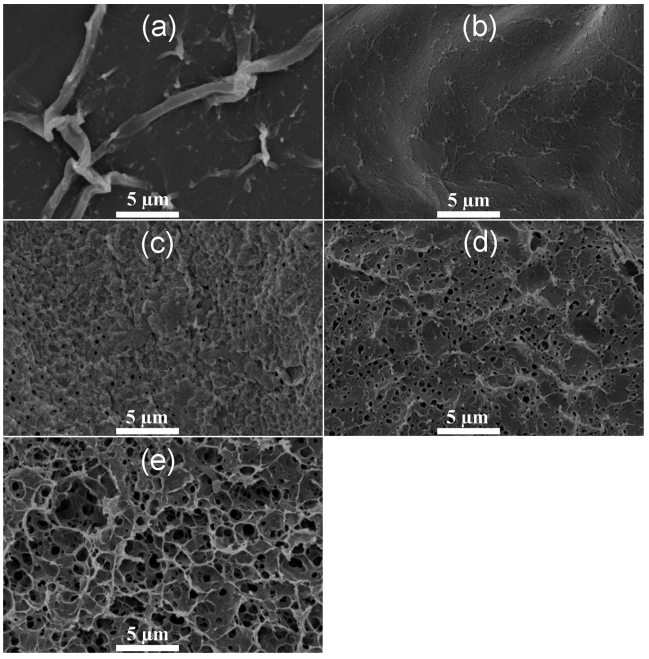

Figure 1. Cross sections of DACbs prior to functionalization. The scanning electron micrographs (SEMs) show the porosity of the beads after freeze-drying. The periodate oxidation of cellulose increases the preservation of a porous structure upon freeze-drying. (a−e) DACbs with different degrees of oxidation: DACb-0, DACb-10, DACb-25, DACb-50, and DACb-100, respectively.

These results might seem to contradict the apparent increase in network density, but these two effects (densification of the hydrated cellulose network and development of larger pores upon freeze-drying) may be correlated. In fact, the partial disruption of crystalline order causes a decrease in susceptibility toward hornification upon drying even at a lower DO (DACb-10), as shown in the scanning electron micrographs (SEMs) in Figure 2, where the stability of the initial and oxidized beads after exposure to solutions at different pH values are compared. Hence, as cellulose hornification is less favorable in DACbs, larger pores are more likely to be preserved upon freeze-drying.

As the enzyme binding step will involve the exposure of DACbs to different pH solutions (see the DACb Enzyme Functionalization section), the stability after exposure at pH 6, 8, and 10 needed to be investigated. Also, the chemical degradation of dialdehyde cellulose under alkaline conditions was expected.[34] Thus, the mechanical stability of DACbs after exposure to different pH solutions was compared. Never-dried single beads were uniaxially compressed with a constant deformation rate (6 μm/s), recording the axial force, which was plotted against the strain percentage. All curves show an exponential behavior characterized by an initial steady increase (elastic region) followed by a sharp increment of the axial force (strain-hardening region) (Figure S2), as expected for cellulose composite gels.[35] The strain values at which the axial force sharply increased (defined here as critical strain) were used to evaluate the mechanical stability. When beads undergo chemical degradation, at high DO and pH values, the critical strain is higher because of the reduced response to stress. Significant differences in the critical strain were observed in DACb-25, DACb-50, and DACb-100 but only at pH 8 and 10 (Figure 3). Hence, the critical strain is dependent on the pH used in the enzyme binding solution and the DO of the material.

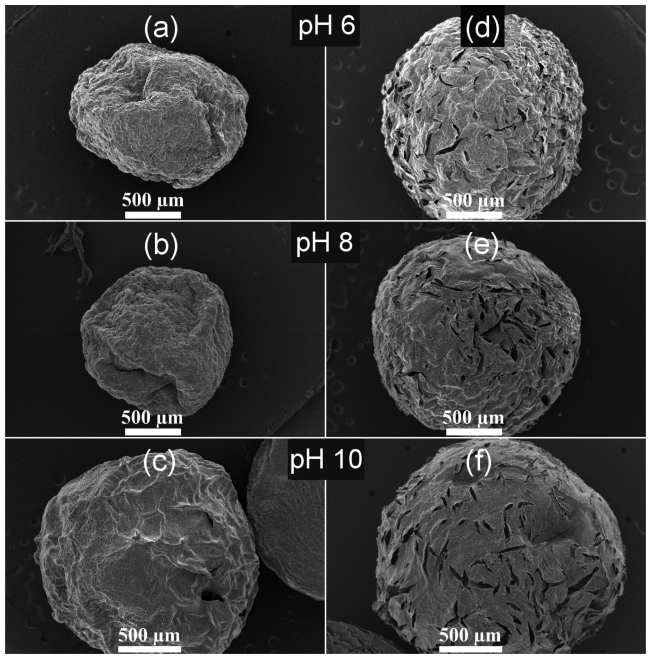

Figure 2. Scanning electron micrographs of beads exposed to different pH solutions: (a−c) Nonoxidized beads (controls) and (d−(f) oxidized DACb-10. The photomicrographs show a different susceptibility to hornification upon freeze-drying. The control beads show a greater degree of cellulose aggregation and collapse compared to the DACb-10 (lowest degree of oxidation after reaction with periodate).

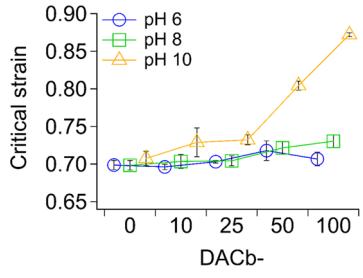

Figure 3. Functionalized bead resistance to mechanical uniaxial compression. The graph shows the differences in critical strain of oxidized beads when exposed at pH 6, 8, and 10 (blue, green, and orange, respectively). The oxidized beads' mechanical resistance to the compression is significantly affected only when exposed to alkaline pH. Error bars represent the standard deviation (n = 3).

DACb Enzyme Functionalization. The bead functionalization consists of two steps: enzyme binding and Schiff base reduction. The enzyme binding (Schiff base formation) was performed by incubating, in static conditions, the DACbs for 18 h in GOx solutions at different concentrations and pH values. Subsequent to binding, the DACbs were transferred to a $NaBH_4$ solution to reduce the imine formed between

https://dx.doi.org/10.1021/acs.biomac.0c01536
Biomacromolecules 2021, 22, 754−762

carbonyl moieties on the cellulose and amino groups of the enzyme. The amount of bound enzyme was evaluated by subtracting the amount of protein in solution left over after incubation (enzyme binding step) and dividing it by the cellulose dry weight. The DO of the DACbs had a significant impact on the amount of enzyme bound at all the pH values used, showing that GOx has higher binding affinity for oxidized cellulose (Table 2).

Table 2. Binding Affinity Constants (K_h) and R^2 of Their Fitting for GOx Bound on DACbs[a]

	pH 6		pH 8		pH 10	
sample code	K_h	R^2	K_h	R^2	K_h	R^2
DACb - 0	21.58	0.97	14.06	0.92	66.55[b]	0.89[b]
DACb - 10	22.92	0.99	17.02	0.92	97.08	0.99
DACb - 25	22.62	0.97	21.23	0.96	105.25	0.97
DACb - 50	30.06	0.93	29.84	0.93	97.34	0.95
DACb - 100	37.35	0.94	42.62	0.91	123.96	0.91

[a]Enzyme was bound on beads with different degrees of oxidation at different pH values to determine the binding affinity constants (K_h). [b]The K_h values for control beads at pH 10 were calculated only using the first three points as the binding curve reaches a plateau.

The shape of DACb-50 and DACb-100 binding curves at pH 6 and 8 showed an increase in the slopes at higher GOx concentrations, suggesting the occurrence of a cooperative adsorption behavior induced by periodate oxidation.[36,37] Cooperative adsorption is often associated with attractive intermolecular interactions, which determine the formation of proteins clusters on the adsorption interface.[38] Similar protein/polymer systems such as immobilized metal Sepharose and histidine-linked methacrylate gels show the same cooperative adsorption behavior expressed as sigmoidal shape isotherm curves.[39,40] However, our isotherm curves only exhibited an initial exponential phase without a plateau (saturation), likely due to the low surface coverage of enzyme on the cellulose.[29]

The major contributing factor for protein binding is the pH. Assuming that covalent binding only occurs between cellulose aldehydes and protein primary amino groups, the expected protein binding should increase as the pH increases.[41] In fact, the highest binding constants for GOx were reached at pH 10 (Figure 4) when the imine formation (Schiff base) between the aldehydes and primary amino groups is more favorable.[42]

The deprotonation of primary amines of GOx (amino terminus and lysine residues, pK_a ~7.7 and ~10.5, respectively) is necessary for the Schiff base formation.[43,44] Thus, the optimum reaction pH strictly depends on the basicity of primary amines present on proteins.

Even at pH 10, the binding curves do not show a plateau except for DACb-0 (nonoxidized control beads), which reaches saturation at higher protein concentrations. The DACb-0 saturation could be attributed to the combination of two factors: (1) the limited number of carbonyls available for Schiff base formation and (2) the protein/protein electrostatic repulsion (GOx pI = 4.2). At pH 6 and 8, binding affinities are less marked. However, *in situ* protein staining (after $NaBH_4$ reduction and washing) shows a higher retention at pH 6 compared to at pH 8, when GOx was bound on beads from the same initial concentration (Figure 5). This suggests that physical interactions and/or unidentified reactions between dialdehyde cellulose and proteins may also have occurred.

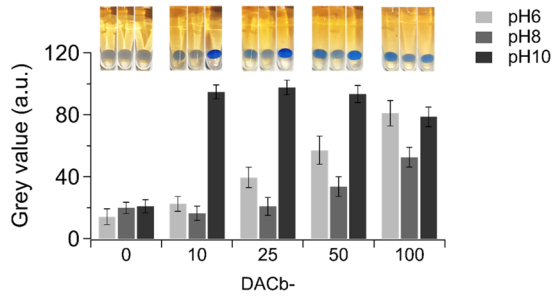

Figure 5. GOx content in DACbs after binding at different pH values and degrees of oxidation. The graph shows the relative GOx content in the beads calculated by extrapolating the gray intensity from the images (insets above) after staining with Coomassie blue (Bradford reagent). The enzyme, dissolved in different buffered solutions at pH 6, 8, and 10, was bound in DACbs with different DO values. The GOx content exhibits different trends after the whole immobilization process (enzyme binding, $NaBH_4$ reduction, and washing). Error bars represent the standard deviation (n = 3).

The functionalization process is therefore highly influenced by pH, which affects not only the mechanical stability (due to the chemical degradation of cellulose) but also the binding efficiency of enzyme immobilization. The degradation of cellulose (also known as peeling) in alkaline conditions is directly proportional to the pH and the DO.[45] In fact, cellulose peeling at pH 10 can be observed in SEM micrographs as DACb structural damage (Figure S3). Nonetheless, the reduction step with $NaBH_4$ after GOx binding should stop the chemical degradation by reducing carbonyl groups into hydroxyl groups,[46] hence preventing further structural damage.

Functionalized Bead Activity. The activity of the enzyme-functionalized beads, prepared at different pH conditions, was measured weekly for three cycles (stored at 4 °C prior each activity cycle). Beads were immersed into an

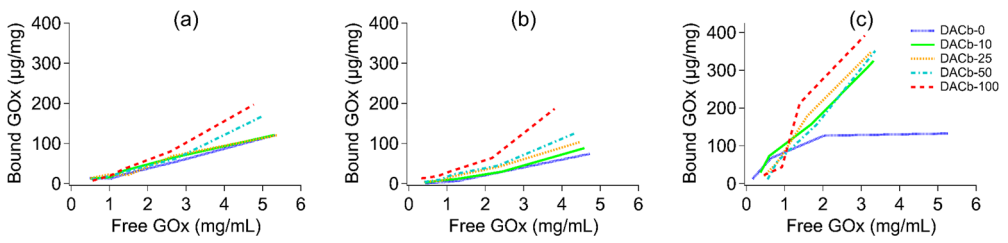

Figure 4. Binding isotherm plots. Binding affinity of GOx in beads with different DO values during the binding step with enzyme solutions buffered at different pH values. Binding at (a) pH 6, (b) pH 8, and (c) pH 10. Each point represents the mean of the independent samples (n = 3).

https://dx.doi.org/10.1021/acs.biomac.0c01536
Biomacromolecules 2021, 22, 754−762

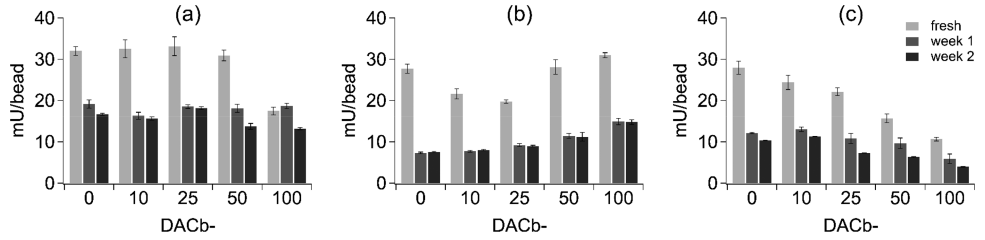

Figure 6. GOx activity upon storage. Activity of beads functionalized at (a) pH 6, pH 8 (b), and pH 10 (c) upon storage at 4 °C. Error bars represent the standard deviation (n = 3).

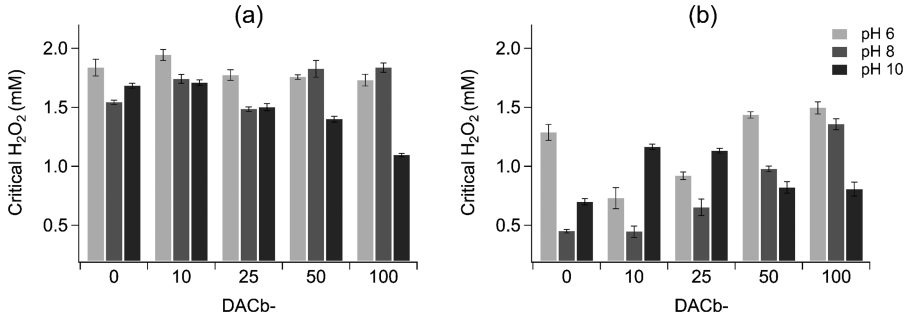

Figure 7. H_2O_2 critical concentration. Concentration of H_2O_2 reached after 24 h of reaction in 10 mL of substrate of (a) freshly functionalized beads and (b) after 14 days of storage at 4 °C. Error bars represent the standard deviation (n = 3).

aqueous buffer at 37 °C (phosphate buffer 0.1 M, pH 6) containing glucose (1 wt %), and the release of H_2O_2 was measured over a time range of 24 h. The H_2O_2 curves showed an initial linear increase (until the first 2.5 h), a curve flattening, and a plateau (Figure S4). The initial linear range was defined as "intrinsic activity", and the maximum H_2O_2 concentration reached after 24 h was defined as "critical concentration". As only a little variation in glucose concentration occurs during the measurement (assuming only enzyme consumption of glucose), it is unlikely that the reduction of the activity was due to substrate depletion. Instead, the curve flattening is attributed to the oxidation of methionine in the active site of the enzyme as a result of H_2O_2 accumulation in the buffer during the reaction.[47,48] To further support this statement, the activity of the functionalized beads that reached the H_2O_2 plateau were assayed again in a substrate-rich medium, but no activity was retained, suggesting that an irreversible enzyme inactivation occurred. Moreover, the H_2O_2 production of the functionalized beads in a larger volume (three times higher: 30 mL) did not show any plateau in H_2O_2 concentration (Figure S5) but only a continuous linear increase over 24 h, suggesting that a lower H_2O_2 concentration (200 μM) did not inhibit the enzyme activity. The intrinsic activity of all freshly prepared beads was significantly higher compared to that of those stored, indicating that enzyme inactivation and/or leakage occurred, although it is not clear which phenomena contributed more (Figure 6).

However, after the first week of storage, a stabilization of the retained activity was observed at pH 6 and 8, suggesting that the main activity loss occurred in the first week of storage after functionalization. The H_2O_2 critical concentration also decreased after the first week of storage but following specific trends, which exhibited a positive impact of the presence of aldehyde moieties on cellulose (Figure 7).

Nonetheless, significant differences among the whole set of samples were observed. The activity values were generally higher in samples where GOx was bound at pH 6 regardless of the DO, while other pH values had opposite trends: increased activity for samples prepared at pH 8 and decreased activity in those prepared at pH 10 was observed as the DO increased. These pH-dependent changes in the activity may be related to the enzyme deactivation due to a partial denaturation during the functionalization process when carried out in alkaline conditions.[49] The critical H_2O_2 concentrations after 1 week selectively decreased, showing a specific trend that confirms that the best performances were achieved in beads where GOx was bound at pH 6. These patterns indicate that a stronger binding (presumably covalent), which was more significant in oxidized beads, might have also affected the enzyme stability against high H_2O_2 concentrations. Nonetheless, the H_2O_2 concentrations reached were high enough to inhibit the growth of the bacterial pathogens tested.

The antimicrobial properties of the functionalized beads were tested by monitoring the impact of the H_2O_2 produced in a 12 mm well punched in the agar of a Petri dish previously inoculated with four different bacterial strains. All experiments were conducted by using the same batch of functionalized beads prepared with the highest DO (DACb-100) where the enzyme (1.4 mg/mL) was bound at pH 6 in order to maximize the H_2O_2 production. To visualize the dose/effect response, 1−3 beads were immersed in the well containing 200 μL of buffered (pH 6) substrate (Figure S6) and coincubated with the bacteria for 24 h. No significant differences were observed for *E. coli* (NCTC 10418) and *P. aeruginosa* (PAO1) in the experiments with 2 or 3 beads, suggesting that the maximum response in terms of inhibition reached its peak with 2 functionalized beads (Figure 8), after which enzyme deactivation may have occurred. MRSA (MRSA252) and *S. aureus* (H560) were less susceptible to H_2O_2, although a significant inhibition compared to the control was observed regardless of the number of beads used.

As reported previously, Gram-positive strains are able to tolerate higher concentrations of H_2O_2 compared to Gram-negative ones. For instance, *S. aureus* H560 has a minimum

https://dx.doi.org/10.1021/acs.biomac.0c01536
Biomacromolecules 2021, 22, 754−762

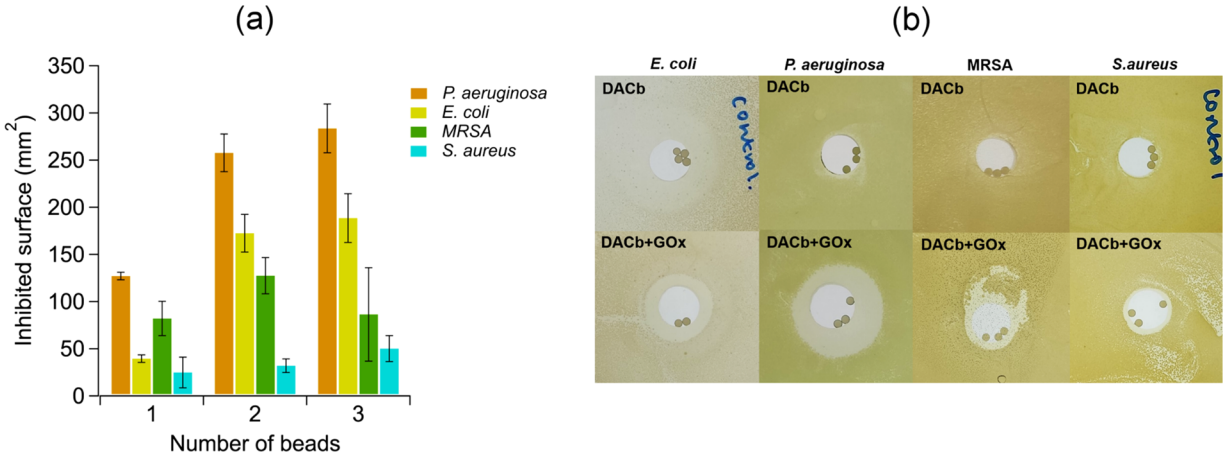

Figure 8. Inhibition halo assay. (a) Graph showing the surface inhibited by the functionalized DACbs in the agar diffusion test. The amount of DACbs used in the test does not influence the surface inhibited in MRSA (MRSA252) and *S. aureus* (HS60), while it increases the surface inhibited in *P. aeruginosa* (PAO1) and *E. coli* (NCTC 10418) between 1 and 2 beads. Error bars represent the standard deviation (n = 3). (b) Above plates represent the DACbs prior GOx functionalization (controls). The plates below represent the DACbs functionalized with GOx. All the bacteria used were inhibited by functionalized DACbs, and the highest inhibition was observed toward *P. aeruginosa* and *E. coli*.

inhibitory concentration (MIC) for H_2O_2 between 1.6 and 3.2 mM and the MIC for *P. aeruginosa* PAO1 is between 0.7 and 1.4 mM. The higher tolerance of Gram-positive bacteria for H_2O_2 can be attributed with the presence of thicker cell-wall peptidoglycan layer, which allows the preservation of cell integrity.[50] In addition, tolerance toward H_2O_2 oxidative stress, in both Gram-positive and -negative bacteria, is also associated with the expression of catalase, an enzyme that is able to neutralize H_2O_2 ($2\ H_2O_2 \rightarrow 2\ H_2O + O_2$).[51,52]

In accordance with other work conducted using standard H_2O_2 solutions,[53,54] the functionalized beads showed growth inhibition in a millimolar range considering the critical H_2O_2 concentrations extrapolated from activity experiments. It is also likely that the H_2O_2 levels reached in the well proximity were lower owing to the diffusion of H_2O_2 into the agarose gel (larger volume). In other words, the antimicrobial effect extrapolated from the agar diffusion experiments could be underestimated. However, the maximization of the H_2O_2 production does not necessarily meet the safety requirements for the design of antimicrobial biomedical devices as wound dressings. In fact, continuous exposure to relatively high concentrations of H_2O_2, i.e., commercial products (~0.9 M) used to irrigate contaminated wounds, may delay tissue healing owing to cytotoxic effects.[12,55] The generation of a lower concentration of H_2O_2 (~60 μM/cm^2) in enzyme-functionalized chitosan mat, designed as wound dressing material, was already sufficient to inhibit the growth of *E. coli* and *S. aureus*.[56] To assess the potential use of the enzyme-functionalized beads as antimicrobial components in biomedical devices, further studies such as *in vitro* biocompatibility assays and *in vivo* wound healing experiments are required.

CONCLUSIONS

The rise of MDR bacteria, caused by inconsiderate use of antibiotics, is one of the biggest threats to public health worldwide. The use of antimicrobial materials to prevent infections is, therefore, important to help to mitigate antibiotic overuse. Here, DACbs were used as solid support for the immobilization of GOx for the release of antimicrobial concentrations of H_2O_2. The porosity and degree of oxidation of the DACbs were easily controlled by modulating the periodate concentration in solution before the oxidation reaction. The degree of oxidation and the pH used for the functionalization process significantly affected the binding affinity of GOx for cellulose, the beads' mechanical properties, and the H_2O_2 release. Alkaline pH was disruptive toward the DACbs and also caused enzyme deactivation. On the contrary, the periodate oxidation of cellulose had a positive effect on the retention of enzyme activity upon immobilization and upon storage at pH 6 and 8. The H_2O_2 released from the functionalized beads was able to inhibit the growth of four different bacterial strains including *P. aeruginosa* and methicillin-resistant *S. aureus*, known to be among the hardest to eradicate in the wound environment.[57] The relatively high H_2O_2 concentrations (≈ 1.8 mM) produced and the prolonged shelf life (at least 2 weeks) make the functionalized beads designed herein a promising and versatile antimicrobial material.

ASSOCIATED CONTENT

Supporting Information

The Supporting Information is available free of charge at https://pubs.acs.org/doi/10.1021/acs.biomac.0c01536.

Figures of changes in bead size and dry weight upon cellulose oxidation, rheological curves for determining resistance to uniaxial compression, SEM images, H_2O_2 kinetic curves, and dose-dependent antimicrobial response of functionalized beads of the agar diffusion test (PDF)

AUTHOR INFORMATION

Corresponding Author

Karen J. Edler − *Department of Chemistry, University of Bath, Claverton Down, Bath BA2 7AY, United Kingdom;* orcid.org/0000-0001-5822-0127; Phone: +44(0) 1225384192; Email: K.Edler@bath.ac.uk

Authors

Davide Califano − *Department of Chemistry and Centre for Sustainable Chemical Technologies, University of Bath, Claverton Down, Bath BA2 7AY, United Kingdom;* orcid.org/0000-0002-9416-2021

https://dx.doi.org/10.1021/acs.biomac.0c01536
Biomacromolecules 2021, 22, 754−762

Bethany Lee Patenall − *Department of Chemistry and Centre for Sustainable Chemical Technologies, University of Bath, Claverton Down, Bath BA2 7AY, United Kingdom*
Marco A.S. Kadowaki − *Department of Chemistry, University of Bath, Claverton Down, Bath BA2 7AY, United Kingdom;* orcid.org/0000-0003-0188-2079
Davide Mattia − *Department of Chemical Engineering, University of Bath, Claverton Down, Bath BA2 7AY, United Kingdom;* orcid.org/0000-0002-7679-4105
Janet L. Scott − *Department of Chemistry and Centre for Sustainable Chemical Technologies, University of Bath, Claverton Down, Bath BA2 7AY, United Kingdom;* orcid.org/0000-0001-8021-2860

Complete contact information is available at: https://pubs.acs.org/10.1021/acs.biomac.0c01536

Notes

The authors declare no competing financial interest.

■ ACKNOWLEDGMENTS

D.C. and B.L.P. would like to thank the University of Bath for PhD studentship funding. M.K. would like to thank the BEIS Rutherford Fund Strategic Partner Grants for a Research Fellowship. The authors also acknowledge funding from the UK EPSRC (EP/P027490/1). Data supporting this article have been made freely available via the University of Bath Research Data Archive system at DOI: https://doi.org/10.15125/BATH-00953.

■ REFERENCES

(1) World Health Organization (WHO). Antimicrobial resistence Fact sheet n° 194. http://www.who.int/news-room/fact-sheets/detail/antibiotic-resistance (accessed 2018-09-25).
(2) World Health Organization (WHO). *Antimicrobial Resistance: Global Report on Surveillance 2014*; 2014.
(3) Spellberg, B.; Blaser, M.; Guidos, R. J.; Boucher, H. W.; Bradley, J. S.; Eisenstein, B. I.; Gerding, D.; Lynfield, R.; Reller, L. B.; Rex, J.; Schwartz, D.; Septimus, E.; Tenover, F. C.; Gilbert, D. N. Combating Antimicrobial Resistance: Policy Recommendations to Save Lives. *Clin. Infect. Dis.* **2011**, *52*, 397−428.
(4) de Oliveira, A.; Pereira, V. C.; Pinheiro, L.; Riboli, D. F. M.; Martins, K. B.; de Lourdes Ribeiro de Souza da Cunha, M. Antimicrobial Resistance Profile of Planktonic and Biofilm Cells of Staphylococcus Aureus and Coagulase-Negative Staphylococci. *Int. J. Mol. Sci.* **2016**, *17*, 1−12.
(5) Frykberg, R. G.; Banks, J. Challenges in the Treatment of Chronic Wounds. *Adv. Wound Care* **2015**, *4*, 560−582.
(6) Elbur, A. I.; Yousif, M. A.; El-Sayed, A. S. A.; Abdel-Rahman, M. E. Prophylactic Antibiotics and Wound Infection. *J. Clin. Diagnostic Res.* **2013**, *7*, 2747−2751.
(7) Wesgate, R.; Grasha, P.; Maillard, J. Y. Use of a Predictive Protocol to Measure the Antimicrobial Resistance Risks Associated with Biocidal Product Usage. *Am. J. Infect. Control* **2016**, *44*, 458−464.
(8) Block, S. S. Sterilants, Disinfectants, and Antiseptics. *Disinfection, sterilization, and preservation*; Lea & Febiger: Philadelphia, PA, 2001; pp 185−204.
(9) Thomas, E. L. Myeloperoxidase, Hydrogen Peroxide, Chloride Antimicrobial System: Nitrogen-Chlorine Derivatives of Bacterial Components in Bactericidal Action against Escherichia Coli. *Infect. Immun.* **1979**, *23*, 522−531.
(10) Linley, E.; Denyer, S. P.; McDonnell, G.; Simons, C.; Maillard, J. Y. Use of Hydrogen Peroxide as a Biocide: New Consideration of Its Mechanisms of Biocidal Action. *J. Antimicrob. Chemother.* **2012**, *67*, 1589−1596.
(11) Zhu, G.; Wang, Q.; Lu, S.; Niu, Y. Hydrogen Peroxide: A Potential Wound Therapeutic Target? *Med. Princ. Pract.* **2017**, *26*, 301−308.
(12) Loo, A. E. K.; Wong, Y. T.; Ho, R.; Wasser, M.; Du, T.; Ng, W. T.; Halliwell, B. Effects of Hydrogen Peroxide on Wound Healing in Mice in Relation to Oxidative Damage. *PLoS One* **2012**, *7*, e49215.
(13) Thallinger, B.; Prasetyo, E. N.; Nyanhongo, G. S.; Guebitz, G. M. Antimicrobial Enzymes: An Emerging Strategy to Fight Microbes and Microbial Biofilms. *Biotechnol. J.* **2013**, *8*, 97−109.
(14) Leskovac, V.; Trivić, S.; Wohlfahrt, G.; Kandrač, J.; Peričin, D. Glucose Oxidase from Aspergillus Niger: The Mechanism of Action with Molecular Oxygen, Quinones, and One-Electron Acceptors. *Int. J. Biochem. Cell Biol.* **2005**, *37*, 731−750.
(15) Tiina, M.; Sandholm, M. Antibacterial Effect of the Glucose Oxidase-Glucose System on Food-Poisoning Organisms. *Int. J. Food Microbiol.* **1989**, *8*, 165−174.
(16) Brady, D.; Jordaan, J. Advances in Enzyme Immobilisation. *Biotechnol. Lett.* **2009**, *31*, 1639−1650.
(17) Homaei, A. A.; Sariri, R.; Vianello, F.; Stevanato, R. Enzyme Immobilization: An Update. *J. Chem. Biol.* **2013**, *6*, 185−205.
(18) Kim, H. J.; Jin, J. N.; Kan, E.; Kim, K. J.; Lee, S. H. Bacterial Cellulose-Chitosan Composite Hydrogel Beads for Enzyme Immobilization. *Biotechnol. Bioprocess Eng.* **2017**, *22*, 89−94.
(19) del Valle, L. J.; Diaz, A.; Puiggali, J. Hydrogels for Biomedical Applications: Cellulose, Chitosan, and Protein/Peptide Derivatives. *Gels* **2017**, *3*, 27.
(20) Liu, Y.; Chen, J. Y. Enzyme Immobilization on Cellulose Matrixes. *J. Bioact. Compat. Polym.* **2016**, *31*, 553−567.
(21) Yee, Y. C.; Hashim, R.; Mohd Yahya, A. R.; Bustami, Y. Colorimetric Analysis of Glucose Oxidase-magnetic Cellulose Nanocrystals (CNCS) for Glucose Detection. *Sensors* **2019**, *19*, 2511.
(22) Calabrese, V.; Califano, D.; da Silva, M. A.; Schmitt, J.; Bryant, S. J.; Hossain, K. M. Z.; Percebom, A. M.; Pérez Gramatges, A.; Scott, J. L.; Edler, K. J. Core−Shell Spheroidal Hydrogels Produced via Charge-Driven Interfacial Complexation. *ACS Appl. Polym. Mater.* **2020**, *2*, 1213−1221.
(23) Tavakolian, M.; Okshevsky, M.; Van De Ven, T. G. M.; Tufenkji, N. Developing Antibacterial Nanocrystalline Cellulose Using Natural Antibacterial Agents. *ACS Appl. Mater. Interfaces* **2018**, *10*, 33827−33838.
(24) Kumari, S.; Chauhan, G. S.; Ahn, J. H.; Reddy, N. S. Bio-Waste Derived Dialdehyde Cellulose Ethers as Supports for α-Chymotrypsin Immobilization. *Int. J. Biol. Macromol.* **2016**, *85*, 227−237.
(25) Zhang, L.; Zhang, Q.; Zheng, Y.; He, Z.; Guan, P.; He, X.; Hui, L.; Dai, Y. Study of Schiff Base Formation between Dialdehyde Cellulose and Proteins, and Its Application for the Deproteinization of Crude Polysaccharide Extracts. *Ind. Crops Prod.* **2018**, *112*, 532−540.
(26) Schneider, C. A.; Rasband, W. S.; Eliceiri, K. W. NIH Image to ImageJ: 25 Years of Image Analysis. *Nat. Methods* **2012**, *9*, 671−675.
(27) Zhao, H.; Heindel, N. D. Determination of Degree of Substitution in Polyaldehyde Dextran by the Hydroxylamine Hydrochloride Method. *Pharm. Res.* **1991**, *8*, 400−402.
(28) Bradford, M. M. A Rapid and Sensitive Method for the Quantitation of Microgram Quantities of Protein Utilizing the Principle of Protein-Dye Binding. *Anal. Biochem.* **1976**, *72*, 248−254.
(29) Oberholzer, M. R.; Lenhoff, A. M. Protein Adsorption Isotherms through Colloidal Energetics. *Langmuir* **1999**, *15*, 3905−3914.
(30) Junglee, S.; Urban, L.; Sallanon, H.; Lopez-Lauri, F. Optimized Assay for Hydrogen Peroxide Determination in Plant Tissue Using Potassium Iodide. *Am. J. Anal. Chem.* **2014**, *05*, 730−736.
(31) Klassen, N. V.; Marchington, D.; McGowan, H. C. E. H2O2 Determination by the I3− Method and by KMnO4 Titration. *Anal. Chem.* **1994**, *66*, 2921−2925.
(32) Kristiansen, K. A.; Potthast, A.; Christensen, B. E. Periodate Oxidation of Polysaccharides for Modification of Chemical and Physical Properties. *Carbohydr. Res.* **2010**, *345*, 1264−1271.

(33) Chavan, V. B.; Sarwade, B. D.; Varma, A. J. Morphology of Cellulose and Oxidised Cellulose in Powder Form. *Carbohydr. Polym.* **2002**, *50*, 41−45.
(34) Knill, C. J.; Kennedy, J. F. Degradation of Cellulose under Alkaline Conditions. *Carbohydr. Polym.* **2003**, *51*, 281−300.
(35) Peng, J.; Calabrese, V.; Ainis, W. N.; Scager, R.; Velikov, K. P.; Venema, P.; van der Linden, E. Mixed Gels from Whey Protein Isolate and Cellulose Microfibrils. *Int. J. Biol. Macromol.* **2019**, *124*, 1094−1105.
(36) Liu, S. Cooperative Adsorption on Solid Surfaces. *J. Colloid Interface Sci.* **2015**, *450*, 224−238.
(37) Muca, R.; Kołodziej, M.; Piatkowski, W.; Carta, G.; Antos, D. Effects of Negative and Positive Cooperative Adsorption of Proteins on Hydrophobic Interaction Chromatography Media. *J. Chromatogr. A* **2020**, *1625*, 461309.
(38) Chatelier, R. C.; Minton, A. P. Adsorption of Globular Proteins on Locally Planar Surfaces: Models for the Effect of Excluded Surface Area and Aggregation of Adsorbed Protein on Adsorption Equilibria. *Biophys. J.* **1996**, *71*, 2367−2374.
(39) Sharma, S.; Agarwal, G. P. Interactions of Proteins with Immobilized Metal Ions: A Comparative Analysis Using Various Isotherm Models. *Anal. Biochem.* **2001**, *288*, 126−140.
(40) Aquino, L. C. L.; Miranda, E. A.; Duarte, I. S.; Rosa, P. T. V.; Bueno, S. M. A. Adsorption of Human Immunoglobuling onto Ethacrylate and Histidine-Linked Methacrylate. *Braz. J. Chem. Eng.* **2003**, *20*, 251−262.
(41) Guisan, J. M. *Immobilization of Enzymes and Cells*; Humana Press: Totowa, NJ, 2013; Vol. *1051*, pp 77−88.
(42) Cordes, E. H.; Jencks, W. P. On the Mechanism of Schiff Base Formation and Hydrolysis. *J. Am. Chem. Soc.* **1962**, *84*, 832−837.
(43) Grimsley, G. R.; Scholtz, J. M.; Pace, C. N. A Summary of the Measured PK Values of the Ionizable Groups in Folded Proteins. *Protein Sci.* **2009**, *18*, 247−251.
(44) Orrego, A. H.; Romero-Fernández, M.; Millán-Linares, M. D. C.; Yust, M. D. M.; Guisán, J. M.; Rocha-Martin, J. Stabilization of Enzymes by Multipoint Covalent Attachment on Aldehyde-Supports: 2-Picoline Borane as an Alternative Reducing Agent. *Catalysts* **2018**, *8*, 333.
(45) Singh, M.; Ray, A. R.; Vasudevan, P. Biodegradation Studies on Periodate Oxidized Cellulose. *Biomaterials* **1982**, *3*, 16−20.
(46) Mateo, C.; Palomo, J. M.; Fernandez-Lorente, G.; Guisan, J. M.; Fernandez-Lafuente, R. Improvement of Enzyme Activity, Stability and Selectivity via Immobilization Techniques. *Enzyme Microb. Technol.* **2007**, *40*, 1451−1463.
(47) Towe, B. C.; Guilbeau, E. J.; Coburn, J. B. In Vivo and in Vitro Deactivation Rates of PTFE-Coupled Glucose Oxidase. *Biosens. Bioelectron.* **1996**, *11*, 791−798.
(48) Cho, Y. K.; Bailey, J. E. Enzyme Immobilization on Activated Carbon: Alleviation of Enzyme Deactivation by Hydrogen Peroxide. *Biotechnol. Bioeng.* **1977**, *19*, 769−775.
(49) Akhtar, M. S.; Bhakuni, V. Alkaline Treatment Has Contrasting Effects on the Structure of Deglycosylated and Glycosylated Forms of Glucose Oxidase. *Arch. Biochem. Biophys.* **2003**, *413*, 221−228.
(50) Mai-Prochnow, A.; Clauson, M.; Hong, J.; Murphy, A. B. Gram Positive and Gram Negative Bacteria Differ in Their Sensitivity to Cold Plasma. *Sci. Rep.* **2016**, *6*, 1−11.
(51) Nakamura, K.; Kanno, T.; Mokudai, T.; Iwasawa, A.; Niwano, Y.; Kohno, M. Microbial Resistance in Relation to Catalase Activity to Oxidative Stress Induced by Photolysis of Hydrogen Peroxide. *Microbiol. Immunol.* **2012**, *56*, 48−55.
(52) Patenall, B. L.; Williams, G. T.; Gwynne, L.; Stephens, L. J.; Lampard, E. V.; Hathaway, H. J.; Thet, N. T.; Young, A. E.; Sutton, M. J.; Short, R. D.; Bull, S. D.; James, T. D.; Sedgwick, A. C.; Jenkins, A. T. A. Reaction-Based Indicator Displacement Assay (RIA) for the Development of a Triggered Release System Capable of Biofilm Inhibition. *Chem. Commun.* **2019**, *55*, 15129−15132.
(53) Bonvillain, R. W.; Painter, R. G.; Ledet, E. M.; Wang, G. Comparisons of Resistance of CF and Non-CF Pathogens to Hydrogen Peroxide and Hypochlorous Acid Oxidants in Vitro. *BMC Microbiol.* **2011**, *11*, 112.
(54) Tonoyan, L.; Fleming, G. T. A.; Mc Cay, P. H.; Friel, R.; O'Flaherty, V. Antibacterial Potential of an Antimicrobial Agent Inspired by Peroxidase-Catalyzed Systems. *Front. Microbiol.* **2017**, *8*, 1−15.
(55) Sierra, H.; Cordova, M.; Chen, C. S. J.; Rajadhyaksha, M. Confocal Imaging-Guided Laser Ablation of Basal Cell Carcinomas: An Ex Vivo Study. *J. Invest. Dermatol.* **2015**, *135*, 612−615.
(56) Bösiger, P.; Tegl, G.; Richard, I. M. T.; Le Gat, L.; Huber, L.; Stagl, V.; Mensah, A.; Guebitz, G. M.; Rossi, R. M.; Fortunato, G. Enzyme Functionalized Electrospun Chitosan Mats for Antimicrobial Treatment. *Carbohydr. Polym.* **2018**, *181*, 551−559.
(57) Turner, N. A.; Sharma-Kuinkel, B. K.; Maskarinec, S. A.; Eichenberger, E. M.; Shah, P. P.; Carugati, M.; Holland, T. L.; Fowler, V. G. Methicillin-Resistant Staphylococcus Aureus: An Overview of Basic and Clinical Research. *Nat. Rev. Microbiol.* **2019**, *17*, 203−218.

https://dx.doi.org/10.1021/acs.biomac.0c01536
Biomacromolecules 2021, 22, 754−762